

Article

Solvent-Free Oxidation of Benzyl Alcohol Derivatives by In Situ Generated Redox Couple Pd(0)/PdO_x Supported on Ceria Nanorods

Seyed Sepehr Moeini ^{1,*}, Simonetta Tuti ¹, Chiara Battocchio ¹, Igor Luisetto ² and Daniela Tofani ^{1,*}¹ Department of Science, “Roma Tre” University, 00146 Rome, Italy² Department of Energy Technologies, Italian National Agency for New Technologies, Energy and Sustainable Economic Development (ENEA), 00123 Rome, Italy

* Correspondence: seyedsepehr.moeini@uniroma3.it (S.S.M.); daniela.tofani@uniroma3.it (D.T.)

Abstract: Benzyl alcohol (BnOH) oxidation to benzaldehyde (PhCHO) is a pivotal industrial reaction. The aerobic oxidation of BnOH in solvent-free conditions is highly compatible with the necessity of low environmental impact. In this research work, palladium oxide (PdO_x) supported on ceria nanorods (CeO₂-NR), was synthesized, and utilized for aerobic solvent-free oxidation of BnOH derivatives to the corresponding aldehydes. The catalyst, PdO_x/CeO₂-NR, was characterized by X-ray diffraction (XRD), field-emission scanning electron microscopy/energy-dispersive spectroscopy (FE-SEM/EDS), N₂ adsorption-desorption analysis, temperature-programmed reduction with hydrogen (H₂-TPR), and X-ray Photoelectron Spectroscopy (XPS), proving that the PdO_x (x > 1) particles were highly dispersed on CeO₂-NR and have a strong interaction with the support. The PdO_x/CeO₂-NR catalyst permitted the aerobic oxidation of various benzyl alcohol derivatives with good conversion, and high selectivity towards the corresponding aldehydes. The presence of electron donating groups (EDG) on the benzylic ring enhanced the reactivity as opposed to the electron withdrawing groups (EWG) which were detrimental for the catalytic activity. During the reaction a partial reduction of the metal produced a Pd(0)/PdO_x/CeO₂-NR redox couple stable in the reaction condition, more reactive and recyclable. Some mechanistic hypotheses are presented.

Keywords: benzyl alcohol; palladium nanoparticles; solvent-free reactions; aerobic oxidation

Citation: Moeini, S.S.; Tuti, S.; Battocchio, C.; Luisetto, I.; Tofani, D. Solvent-Free Oxidation of Benzyl Alcohol Derivatives by In Situ Generated Redox Couple Pd(0)/PdO_x Supported on Ceria Nanorods. *Catalysts* **2023**, *13*, 5. <https://doi.org/10.3390/catal13010005>

Academic Editor: Dinesh Kumar

Received: 16 November 2022

Revised: 12 December 2022

Accepted: 16 December 2022

Published: 21 December 2022



Copyright: © 2022 by the authors. Licensee MDPI, Basel, Switzerland. This article is an open access article distributed under the terms and conditions of the Creative Commons Attribution (CC BY) license (<https://creativecommons.org/licenses/by/4.0/>).

1. Introduction

The selective oxidation of benzyl alcohol (BnOH) to benzaldehyde (PhCHO) is considered a critical organic transformation either for the importance of PhCHO as a fine chemical and for the environmental implications that the reaction can bring about [1,2].

To avoid toxic and pollutant oxidants, various studies have focused the attention on the use of oxygen as an environmentally benign oxidizing agent. This kind of reaction could be effectively catalyzed by noble metals, such as gold, ruthenium, or palladium, that are often nano dispersed on less expensive supporting materials such as ceria, silica, and carbon [3]. Recent literature has evidenced a strong influence on the catalytic activity of metal dispersion [4], support morphology [5,6], and reaction conditions (concentration, temperature, solvent) [2]; thus, the preparation of the support and the method of dispersion of the metal could play a pivotal role in the efficiency and selectivity of the reaction.

In addition, due to the cost and toxicity of many organic solvents, omitting their usage can be a further attractive improvement to the environmental impact of the reaction. This could be done either using water [7] or the alcohol substrate itself as the solvent as proposed by Wang [8] and more recently by Xia [9], Li [10], and others [11,12].

At the same time, in-depth studies have been devoted to elucidating the catalytic mechanism of oxidation of benzyl alcohol by metals supported on nanoparticles in order to avoid secondary products such as toluene and benzoic acid [2,13–18]. In the case of Pd(0),

various competing reaction pathways were proposed depending on temperature, substrate, and oxygen concentration. The prevalence of one or the other leads to the main product with a different percentage of secondary derivatives [13].

Recently, researchers have analyzed the BnOH oxidation mechanism under solvent free conditions [14]. From a mechanistic point of view, the absence of solvent, i.e., the use of polar protic BnOH alone, may have a massive effect, considering that these reactions are normally carried out in toluene or aromatic aprotic solvents. Xin et al. observed that, using Pd on crystalline nanoporous CeO₂ in solvent free conditions, BnOH derivatives with electron-donating groups (EDG) on the aromatic ring were oxidized less than BnOH itself (18.63% for 4-methylbenzyl alcohol, 11.12% for 4-methoxybenzyl alcohol, and 26.60% for BnOH), while a slightly higher percentage of the benzylic alcohol with 4-nitro electron-withdrawing group (EWG) was converted to the aldehyde derivative (27.13% of 4-nitrobenzyl alcohol) [4]. These results contrast with the studies of Xu et al. [19], for the oxidation of similar substrates catalyzed by Pd supported on mesoporous carbon, using toluene as solvent. As a matter of fact, Xu et al. observed that addition of a nitro group decreased the alcohol conversion (54% in 4 h), while EDG resulted in higher conversion of alcohol compared to BnOH (92% and 93% in 4 h for 4-methyl and 4-methoxy derivatives, respectively).

The oxidation state of palladium plays a crucial role in the catalytic activity and the reaction mechanism [2,5]. Many research works focused on Pd(0) catalysts due to high reactivity [20] but the metallic palladium could be oxidized because of the oxygen or an oxidizing environment such as nanostructured ceria support [21], so maintaining the palladium in reduced form on support materials with high oxygen reservoir capacity such as ceria nanomaterials is a difficult task [22]. Therefore, preparing the catalyst with the oxide species of palladium might be easier to control and lead to a more stable catalyst compared to Pd(0) counterparts. In addition, the more reactive Pd(0) species can be produced from the palladium oxide species during the solvent-free oxidation of alcohols because the high concentration of alcohol can initiate the palladium reduction, as observed by Jürgensen et al., for the reduction of PdO supported on TiO₂ in presence of propyl alcohol at temperatures higher than 90 °C [23].

In this work, palladium oxide (PdO_x) supported on ceria nanorods (CeO₂-NR) was prepared by a synthetic procedure slightly different than our previously published method [5], due to a change of palladium precursor (see Section 3. Materials and Methods). The catalyst was characterized and compared with the one previously produced, showing different chemical and physical properties. The new PdO_x/CeO₂-NR was then tested for solvent-free oxidation of various BnOH derivatives substituted in the aromatic ring with EDG and EWG groups. Some mechanistic hypotheses are proposed based on the findings of catalyst analysis after reaction and the results of oxidation of different BnOH derivatives.

2. Results and Discussion

In this work the palladium precursor used for wet impregnation was a commercial solution of Pd(NO₃)₂ (see Section 3. Materials and Methods). These conditions probably produced a more homogeneous deposition of the palladium on the ceria surface, facilitating a better oxidation during the calcination process. Only one palladium oxide species was detected in the sample as discussed in the X-ray photoelectron spectroscopy (XPS).

2.1. Characterization

X-ray Diffraction (XRD) pattern of the CeO₂-NR support showed the reflections of pure cubic fluorite CeO₂ at 2θ about 28.5° (111), 33.1° (200), 47.5° (220), 56.4° (311), 59.2° (222), 69.5° (400), and 79.1° (420), (Joint Committee on Powder Diffraction Standards (JCPDS) card 81-0792) (Figure 1). The cubic cell size, “a” parameter, was 5.408 Å, and the average crystallite size calculated from the Size–Strain plot (Figure S1a) was about 13 nm (Table 1). The XRD pattern of the PdO_x/CeO₂-NR sample showed only the reflections assigned to CeO₂, with the same position and nearly the same full width at half maximum (FWHM)

of CeO₂-NR support, corresponding to an average crystallite dimension of about 12 nm (Figure S1b); an unvaried size cell of 5.405 Å indicates that the Pd-loading process did not affect the crystallite structure (Figure 1, Table 1), excluding the solution of Pd into CeO₂ crystal lattice. The absence of the PdO_x diffractions is due to the low content. However, the most intense peak of PdO is expected at 33.8° (101), very close to the (200) reflection of CeO₂, and so it might be hardly revealed.

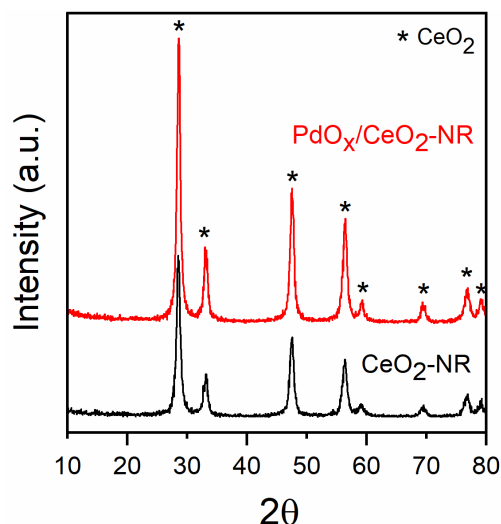


Figure 1. X-ray diffraction (XRD) patterns of the CeO₂-NR and PdO_x/CeO₂-NR samples.

Table 1. Crystallite size and cell parameters of CeO₂ and textural properties of samples.

Sample	CeO ₂ Crystallite Size (nm)	CeO ₂ Cell Size (Å)	Surface Area (m ² g ⁻¹)	Average Pore Diameter (nm)	Total Pore Volume (cm ³ g ⁻¹)
CeO ₂ -NR	13	5.408 ± 0.001	94	19	0.40
PdO _x /CeO ₂ -NR	12	5.405 ± 0.003	68	13	0.26

The morphology and chemical composition of the pure ceria support and the PdO_x/CeO₂-NR catalyst were analyzed by field-emission scanning electron microscopy/energy-dispersive spectroscopy (FE-SEM/EDS). The FE-SEM images of CeO₂-NR and PdO_x/CeO₂-NR showed a rod-like morphology (length to width ratio above 5 with a uniform and well-developed structure (Figure 2)), suggesting that palladium deposition did not affect the morphology of the ceria support. No evidence of palladium particles was observed, suggesting that the metal oxide particles could be well-dispersed. The EDS analysis of PdO_x/CeO₂-NR measured 2.01 ± 0.07 wt.% of palladium in the sample, in good agreement with the nominal 2.00 wt.% metal content.

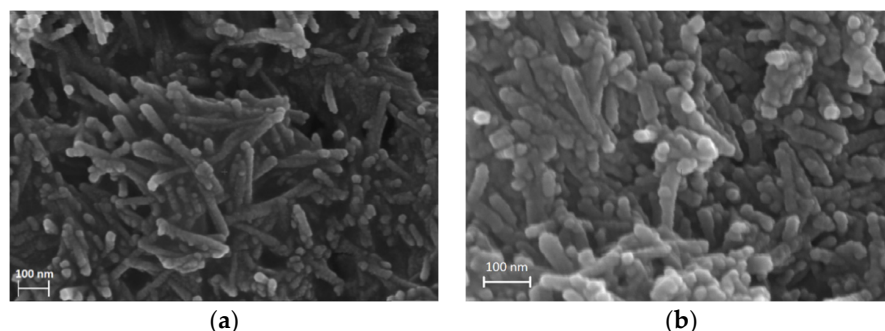


Figure 2. Field-emission scanning electron microscopy (FE-SEM) of (a) CeO₂-NR and (b) PdO_x/CeO₂-NR.

Brunauer–Emmett–Teller (BET) surface area of pure $\text{CeO}_2\text{-NR}$ was $94 \text{ m}^2 \text{ g}^{-1}$. The palladium deposition caused a decrease of the support surface area down to $68 \text{ m}^2 \text{ g}^{-1}$ (Figure 3 and Table 1).

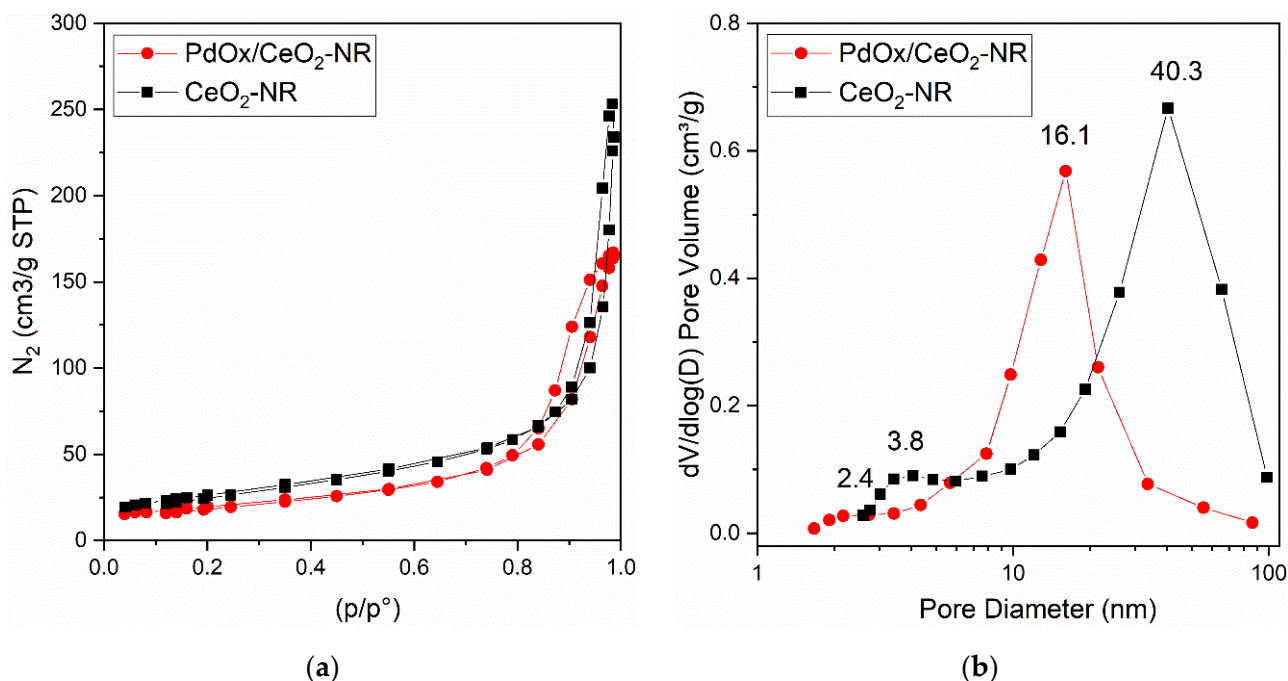


Figure 3. Brunauer–Emmett–Teller (BET) analysis of the $\text{CeO}_2\text{-NR}$ and $\text{PdO}_x/\text{CeO}_2\text{-NR}$ samples: (a) nitrogen adsorption–desorption isotherms as a function of the relative pressure p/p° ; (b) Barrett–Joyner–Halenda (BJH) pore size distributions (PSD).

$\text{CeO}_2\text{-NR}$ pure support and $\text{PdO}_x/\text{CeO}_2\text{-NR}$ catalyst both showed N_2 adsorption–desorption curves Type V, with hysteresis loops H1-Type for $\text{CeO}_2\text{-NR}$ and H2(b)-Type for the $\text{PdO}_x/\text{CeO}_2\text{-NR}$ catalyst by IUPAC classification [24]. Both these features are characteristic of a well-developed and uniform mesoporous morphology (Figure 3a). In addition, the H2(b)-Type shape is associated with the blocking of pores, with a large distribution of neck widths. Barrett–Joyner–Halenda (BJH) pore size distributions (PSD) of both samples were in the range of 1.5–100 nm, centered at 40.3 nm for pure $\text{CeO}_2\text{-NR}$, and at 16.1 nm for the $\text{PdO}_x/\text{CeO}_2\text{-NR}$ catalyst (Figure 3b). The corresponding average pore diameter was 19 nm for pure $\text{CeO}_2\text{-NR}$ and decreased down to 16 nm for the $\text{PdO}_x/\text{CeO}_2\text{-NR}$ sample; in agreement, the corresponding total pore volume decreased from 0.40 down to $0.26 \text{ cm}^3 \text{ g}^{-1}$ (Table 1). As expected, the addition of palladium oxide on the surface causes a decrease of surface area, pore size, and pore volume of the material, suggesting a partial occlusion of ceria pores.

The XPS analysis of $\text{PdO}_x/\text{CeO}_2\text{-NR}$ showed that there was only one Pd species on the surface of ceria, with Pd $3d_{5/2}$ component at almost 338 eV binding energy (BE; Figure 4), a binding energy value indicative of oxidized palladium (PdO_x , $x > 1$), similar to the PdO_x component observed in $\text{PdO}_x/\text{CeO}_2\text{-NR}$ in our previous work [5]. However, here the PdO_x is the only palladium species detected on the $\text{CeO}_2\text{-NR}$, whereas, in the catalyst of our previous work, 10% PdO was present as well. In addition, the palladium atomic ratio i.e., $\text{Pd}/(\text{Pd} + \text{Ce})$ on the surface of $\text{PdO}_x/\text{CeO}_2\text{-NR}$ was 10.3%.

Ce3d spectra of the sample is as expected, extremely complicated, due to the different components arising by Ce(III) and Ce(IV) ions. By following a peak-fitting procedure, five spin orbit pairs related to Ce3d were individuated, and the resulting components were associated to the different ions by comparison with literature data [25,26], as reported in detail in Table 2. The Ce(III)/Ce(IV) atomic ratio was estimated at about 1:1 (Ce(III)

percentage = 52%, Ce(IV) percentage = 48%), significantly higher than the 24% Ce(III) of the catalyst of our previous study [5], suggesting enhanced oxygen vacancy on the support.

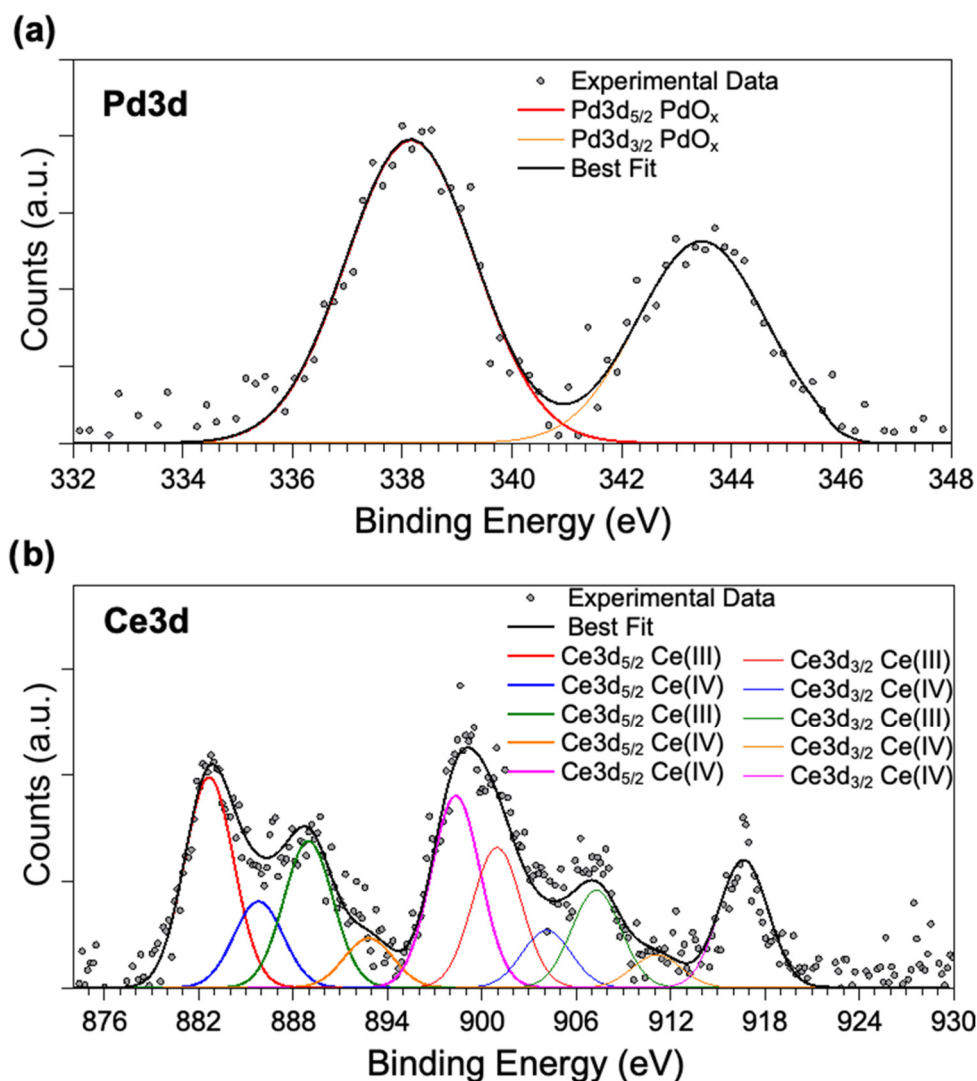


Figure 4. X-ray photoelectron spectroscopy (XPS) spectra of (a) Pd 3d region, (b) Ce 3d region for PdO_x/CeO₂-NR.

Table 2. Binding energy (BE) and full width at half maximum (FWHM) values and proposed assignments for the PdO_x/CeO₂-NR catalyst.

Signal	BE (eV)	FWHM (eV)	Assignment
Ce3d _{5/2}	882.59	3.87	Ce(III)
-	885.20	3.87	Ce(IV)
-	887.24	3.87	Ce(III)
-	891.14	3.87	Ce(IV)
-	898.72	3.87	Ce(IV)
Pd3d _{5/2}	338.16	2.76	PdO _x

H₂-TPR experiment was performed to obtain information about the homogeneity of PdO_x species on the surface, and to test the redox properties of Ce(III)/Ce(IV) couple, that determines the oxygen storing capacity of the ceria surface. The reduction was conducted from 40 °C to 500 °C, to limit the sintering of CeO₂ and Pd at higher temperatures. The pure support CeO₂-NR showed an intense reduction peak, starting at about 250 °C with a

maximum at about 450 °C, assigned to the reduction of Ce(IV) to Ce(III) on the surface of ceria (Figure 5). The total consumption of hydrogen corresponded to a ratio of exchanged electrons for Ce atom (e^-/Ce) equal to 0.178, related to the reduction of 17.8% of the nominal content of CeO_2 (Table 3). The $\text{PdO}_x/\text{CeO}_2\text{-NR}$ catalyst showed a hydrogen consumption below 60 °C, and an intense broad peak in the range of 100–300 °C, with two components at 140 °C and 215 °C, and a very weak hydrogen consumption in the range of surface ceria reduction (250–500 °C) (Figure 5). The TPR profile of $\text{PdO}_x/\text{CeO}_2\text{-NR}$ did not show a negative peak, observed by many authors in the temperature range of 50–100 °C due to the decomposition of PdH_x species [5,27]. The formation of PdH_x species has been related to the presence of larger Pd particles [27,28].

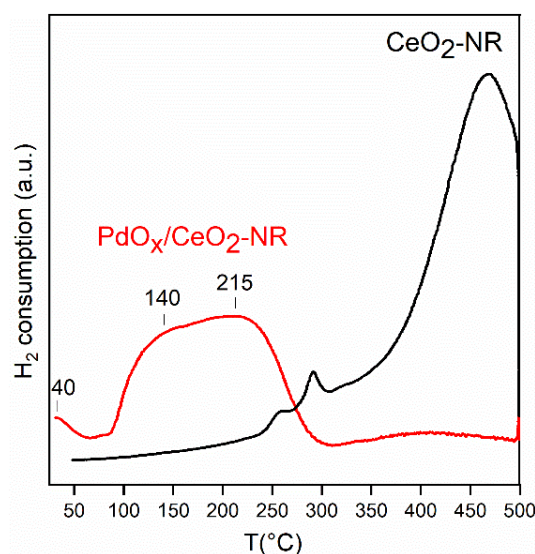


Figure 5. Temperature programmed reduction (H_2 -TPR) profiles of the $\text{CeO}_2\text{-NR}$ and $\text{PdO}_x/\text{CeO}_2\text{-NR}$ samples.

Table 3. Redox properties by H_2 -TPR analysis: hydrogen consumption and reduction degree of Pd and Ce.

Sample	H_2 Consumption in Range 40–300 °C ($\mu\text{mol g}^{-1}$)	e^-/Pd (mol/mol)	H_2 Consumption (T Range) ($\mu\text{mol g}^{-1}$)	Ce(III) (%)
$\text{CeO}_2\text{-NR}$	-	-	518 (250–500 °C)	17.8
$\text{PdO}_x/\text{CeO}_2\text{-NR}$	175	1.87	19 (300–500 °C)	0.64

The reduction temperatures reported in the literature for $\text{PdO}_x/\text{CeO}_2$ catalysts with a similar Pd loading are in a very wide temperature range, depending on the preparation method and on the calcination temperature. PdO_x reduction was observed at low temperature: in the range (−13)–(−23) °C [27], 30–64 °C [29,30], 20–160 °C [31], 50–200 °C [32], and 130–257 °C [28,33]. The presence of several peaks at different temperatures was attributed by the authors to the reduction of PdO_x species with different support interaction and/or different particle dimensions, but in the latter case there is no total agreement between the authors. Based on the literature data, the three peaks at about $T < 60$ °C, $T = 140$ °C, and $T = 215$ °C, observed for $\text{PdO}_x/\text{CeO}_2\text{-NR}$ of this study, are attributed to the reduction of PdO_x species with increasing dispersion and increasing strength of the interaction with the support [32], and to the reduction of the Ce(IV) to Ce(III) promoted by palladium at lower temperature. The total consumption of hydrogen in the range 40–300 °C corresponds to a ratio of exchanged electron for palladium atom $e^-/\text{Pd} = 1.87$. The very weak H_2 consumption in the range 300–500 °C, corresponds to the reduction of only about 0.64% of the nominal content of CeO_2 to Ce(III) (Table 3). Furthermore, it is important to consider the

occurrence of the hydrogen spill-over phenomena, likely present on noble metal supported on ceria, causing difficulty in peak attribution and hydrogen consumption larger than the stoichiometric amount. The e^-/Pd value lower than two, together with the profile shape in range 40–60 °C, that evidences a hydrogen consumption at 40 °C, both suggest that a fraction of PdO_x was reduced during the initial thermal conductivity detector (TCD) stabilization step at $T = 40$ °C, consisting of a H_2 flow through the sample for 40 min. The TPR characterization shows that the Pd strongly influences the redox properties of ceria surface, promoting the ceria reduction at very lower temperature, lower than that observed in the previously studied Pd-CeO₂-NR sample [5], and reinforcing the evidence that PdO_x is highly dispersed and strongly interacting with the surface.

2.2. Catalytic Tests

In the literature, BnOH oxidation in solvent free conditions on various supported Pd(0) nanocatalysts gave different results from the 19.8% conversion (97.8% selectivity) on layered hydroxides [10] to the 89.9% conversion (63.7% selectivity) of functionalized crystalline Pd nanoparticles on nanoporous CeO₂ [8].

Different studies have evidenced that Pd(0) is more reactive as a catalyst than PdO [20]. However, in presence of CeO₂, Pd(0) can be rapidly oxidized to PdO by oxygen [34]. Considering that in solvent-free reactions the high concentration of alcohol can initiate the reduction of the palladium oxide, as in presence of propyl alcohol at temperatures higher than 90 °C [23], the catalyst prepared in this research was not pre-reduced but used in oxide form. The oxidation reactions (Table 4) were performed in solvent-free conditions, in presence of PdO_x/CeO_2 -NR as catalyst and benzophenone as internal standard, keeping the temperature at 100 °C (unless otherwise specified) and the air flow at 5 mL min⁻¹ for 18 h. The reactants were identified by gas chromatography-mass spectrometry (GC-MS) and were quantified via high-performance liquid chromatography (HPLC). In the blank experiment in which CeO₂-NR was used as catalyst, no BnOH conversion occurred after 18 h. The results of the oxidation of BnOH derivatives are reported in Table 4. BnOH conversion was 50% with 93% PhCHO as product. Neither toluene nor benzoic acid were detected, and the only secondary product was benzyl benzoate, probably derived from the acid esterification by concentrated BnOH.

Table 4. Substrates and reaction results of catalytic oxidation of benzyl alcohol (BnOH) derivatives and 4-(benzyloxy)phenol.

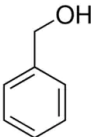
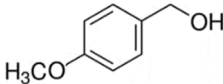
Entry	Reactant	Conversion (%)	Aldehyde Selectivity (%)
1		50	93
2		70	86

Table 4. Cont.

Entry	Reactant	Conversion (%)	Aldehyde Selectivity (%)
3		46	97
4		52	90
5		<3	>97
6		66	81
7		<3	>97
8		62	94
9		>97	<3
10		<3	>97
11		<3	>97
12		31	<3

Reaction conditions: 5 mmol substrate, 5 mg PdO_x/CeO₂-NR, 5 mL min⁻¹ air flow, 18 h at 100 °C (exceptions: entry 9 and 12 at 130 °C). Benzophenone was used as an internal standard. Conversion and selectivity are calculated using high-performance liquid chromatography (HPLC).

The catalytic activity of PdO_x/CeO₂-NR was also analyzed in the presence of various BnOH derivatives. In the same reaction conditions, presence of EDG on the para position of the aromatic ring led to an increase in substrate conversion with a slight decrease in the selectivity towards the aldehydic product. In case of 4-methoxybenzyl alcohol and

4-methylbenzyl alcohol (entry 2 and 6, Table 4), the conversion raised up to 70% and 66% respectively, with 86% and 81% selectivity towards the corresponding 4-methoxy- and 4-methylbenzaldehyde. On the contrary, in the oxidation of 4-phenoxybenzyl alcohol, a decrease in conversion and an improvement of selectivity was observed (62% and 94%, respectively, entry 8, Table 4). This last result could be attributable to the presence of a second aromatic ring that could compete with the adsorption of the benzyl ring on the active sites of the catalyst surface.

In the case of 3-methoxybenzyl alcohol (entry 3, Table 4) the reactivity decreases in comparison with the reference 4-methoxy isomer. It can be assumed that the stabilizing contribution to the rate-determining transition state is more relevant if the EDG is in a resonance position. With 3,4-dimethoxybenzyl alcohol the two different effects produced a small decrease in conversion respect to 4-methoxyderivative, maintaining the high selectivity towards the aldehydic product (entry 4, Table 4).

If the substituent is in the ortho position, as in the 2-methoxy- and 2-methyl-derivatives, the steric hinderance of the group seemed more influential than the electron donating effect; therefore, the substrate hardly reacted (<3% conversion, entry 5 and 7, respectively, Table 4). These effects of hinderance have already been highlighted by Kara et al. [35] in the oxidation of 4-methoxy- and 2-methoxybenzyl alcohol using perlite/V₂O₅ nanospheres catalyst with yields of 92% and 70% respectively.

In the oxidation of highly reactive 4-hydroxybenzyl alcohol (at 130 °C), the fast decrease of the substrate concentration did not lead to a concurrent enhancement of the concentration of aldehydic product (entry 9, Table 4). Instead, in the HPLC analyses a big peak appeared at higher retention times. Probably, in solvent-free conditions, a parallel reaction could have occurred between the highly concentrated unreacted substrate and the corresponding aldehyde leading to polymerization products, easily visible after purification as sticky materials, which could result from the acetalization process.

Acidic work-up conditions used to revert the formation of these secondary products permitted the isolation of a derivative that, after partial chromatographic purification and GC-MS analysis, proved to be a mixture of 4-hydroxybenzaldehyde and a dimer.

On the contrary, the oxidation of BnOH derivatives containing EWG were unsuccessful by PdO_x/CeO₂-NR, as observed for 4-nitrobenzyl alcohol and methyl(4-hydroxymethyl)benzoate, with less than 3% conversion (entry 10 and 11, Table 4).

In the end, 4-(benzyloxy)phenol (entry 12, Table 4) as a model compound of lignin structures was tried with PdO_x/CeO₂-NR in solvent free conditions at 130 °C. The HPLC analysis showed that 31% of the substrate was converted after 18 h. A small amount of PhCHO and bigger amounts of two other oxidation products were detected, suggesting the partial breakage of the C–O bond. This last result is particularly significative because it is generally difficult to break the ether bond at ambient pressure which is extremely useful in lignin degradation and its waste valorization [36]. Further studies are underway to fully identify the products and extend the use of this catalyst in lignin depolymerization.

2.3. Mechanistic Aspects

Even if many research groups have studied the mechanism of BnOH oxidation [2], only a few articles have dealt with the effect of EWG or EDG on the reactivity [4,19,35,37,38]. The reactions performed with different benzyl alcohol derivatives help to hypothesize on the reaction mechanism. In general, the effect of the substituents is more evident in heterolytic reactions where an ion stabilizing effect is more influential. In solvent-free reactions with PdO_x/CeO₂-NR as catalyst, the use of PdO_x and high concentration of alcohol produced an environment more polar than the toluene solvent generally used in similar reactions. BnOH is absorbed on PdO_x through the dissociation of its OH bond as already demonstrated by various research groups [2,13]. Then, the oxygen acts directly as hydrogen abstractor producing the oxidation to aldehyde of the alkoxide bound and the concurrent reduction of palladium to a lower oxidation state after the release of the adsorbed hydrogen as water [39]. This is observable during the reaction where the catalyst

color changes from light brown of the $\text{PdO}_x/\text{CeO}_2$ to a dark grey due to the presence of $\text{Pd}(0)$ (Figure S2). In fact, the massive amount of the benzylic alcohol derivative present in the reaction can facilitate the in situ reduction of PdO_x to $\text{Pd}(0)$ as previously demonstrated by Jürgensen in BnOH oxidation by PdO/TiO_2 catalyst [23]. XPS measurements carried out on the “used” $\text{PdO}_x/\text{CeO}_2$ -NR sample, recovered from the catalytic reaction on BnOH , confirmed this hypothesis, showing the presence of approximately 30% reduced $\text{Pd}(0)$ atoms, assigned to the low BE signal ($\text{Pd } 3d_{5/2}$ BE = 335.42 eV) in Figure 6. The signal at higher BE is attributed to unperturbed PdO_x species [40].

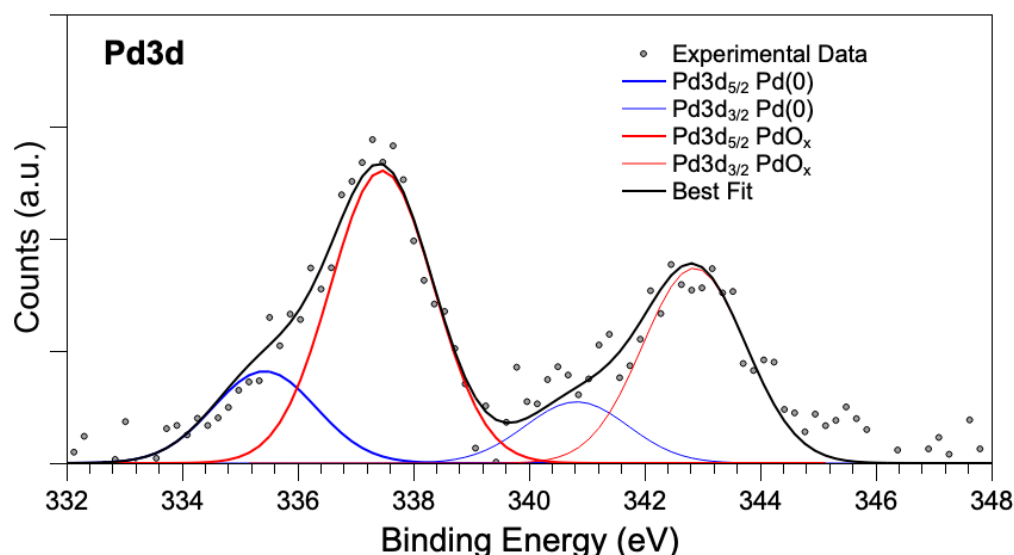


Figure 6. Pd 3d XPS spectrum of “used” $\text{PdO}_x/\text{CeO}_2$ -NR. The catalyst was recovered after BnOH oxidation, washed with acetonitrile, dried under vacuum at lab temperature, and kept in a sealed container before XPS analysis.

The contemporary presence of the more reactive produced $\text{Pd}(0)$ then activates a faster catalytic process in which $\text{Pd}(0)$ and PdO_x can catalyze synergistically the benzyl alcohol oxidation as recently demonstrated by Zhe Wang et al. on a similar ceria-based catalyst [39].

The oxygen flow partially re-oxidizes the $\text{Pd}(0)$ to PdO_x leading to an equilibrium between the two redox species. It is likely that CeO_2 -NR facilitates this equilibrium.

The recyclability tests performed on the catalyst (Table 5) not only confirmed the stability of the $\text{Pd}(0)/\text{PdO}_x$ redox couple on CeO_2 -NR but underlined the increased reactivity of the catalyst used in subsequent runs.

Table 5. Recyclability test of $\text{PdO}_x/\text{CeO}_2$ -NR catalyst in BnOH to benzaldehyde (PhCHO) oxidation.

Reaction Cycle	BnOH Conversion %	PhCHO Selectivity %
1	51	94
2	61	89
3	60	90

Reaction conditions: 5 mmol substrate, 5 mg $\text{PdO}_x/\text{CeO}_2$ -NR, 5 mL min^{-1} air flow, 18 h at 100 °C. Conversion and selectivity are calculated using HPLC.

As regards the different reactivity of the BnOH derivatives with respect to the data of Xin et al. [4], this could be attributed to the presence of PdO_x catalyst instead of only metallic palladium.

Furthermore, when compared with other solvent free processes [4,38,41], the higher $\text{PdO}_x/\text{CeO}_2$ -NR reactivity difference in substrates containing EDG on the aromatic ring as compared to those with EWG could be attributed to an ionic transition state facilitated by the presence of palladium oxide and the polar environment. In these conditions, groups

that can donate electrons during the rate determining hydride abstraction enhance the BnOH conversion while electron withdrawing groups on the aromatic ring strongly slow down the process.

3. Materials and Methods

Benzyl alcohol $\geq 99\%$, 4-methoxybenzyl alcohol 98%, 2-methoxybenzyl alcohol 99%, 3-methoxybenzyl alcohol 98%, 3,4-dimethoxybenzyl alcohol 96%, 2-methylbenzyl alcohol 98%, 4(benzyloxy)phenol 98%, palladium(II) nitrate solution (10 wt.% in 10 wt.% nitric acid; 99.999% trace metal), cerium(III) nitrate hexahydrate ($\geq 99.0\%$ trace metal basis), acetonitrile (for HPLC, gradient grade, $>99.9\%$), ethanol (for HPLC, $\geq 99.8\%$), and Whatman[®] quantitative filter paper (ashless, Grade 42) were purchased from Sigma Aldrich (Darmstadt, Germany). 4-methylbenzyl alcohol 99%, 4-phenoxybenzyl alcohol 97%, 4-hydroxybenzyl alcohol 99%, 4-nitrobenzyl alcohol 99%, methyl(4-hydroxymethyl)benzoate 99% were bought from Alfa Aesar (Kandel Germany). Ethyl acetate, diethyl ether, NaOH (for analysis-ACS-ISO) were purchased from Carlo Erba (Cornaredo, Italy). Benzophenone ($>99\%$) was bought from Fluka (Buchs, Switzerland).

The PdO_x/CeO₂-NR catalyst was prepared according to our previously published work [5] but with changing the palladium precursor from Alfa Aesar solid Pd(NO₃)₂·2H₂O solubilized in HNO₃ solution to Sigma Aldrich Pd(NO₃)₂ solution. The CeO₂-NR was prepared by hydrothermal treatment of Ce(NO₃)₃·6H₂O at high pH and at 100 °C. Cerium nitrate hexahydrate, 1.300 g, was dissolved in 20.0 mL distilled water and then mixed in a Teflon bottle with an alkali solution of 14.400 g sodium hydroxide in 40.0 mL distilled water. After 30 min stirring, the Teflon bottle was inserted in a stainless-steel autoclave vessel and put in an oven at 100 °C for 24 h. Then the obtained precipitate was vacuum filtered, washed with distilled water and ethanol. To fully evaporate the remaining solvent, the solid was left in the oven overnight at 120 °C. Finally, the prepared solid was uniformly milled and then calcined at 400 °C for 5 h, resulting in the light-yellow ceria powder (Figure S2a). The prepared ceria support was then used in a wet impregnation process aiming at the deposition of 2.00 wt.% palladium. For this, 10.0 mL of Pd(NO₃)₂·2H₂O commercial solution was added drop by drop to 1.000 g of CeO₂-NR in a 50 mL flask maintaining the temperature at 60 °C for 2 h under stirring. Then, using a rotavapor, the water was removed and the solid was dried in the same drying condition of ceria support. Finally, the dried solid was milled and calcined at 500 °C for 5 h to acquire the PdO_x/CeO₂-NR with light brown color (Figure S2b).

XRD patterns were recorded using a Scintag X1 diffractometer (Scintag Inc., San Francisco, CA, USA) equipped with a Cu K α ($\lambda = 1.5406 \text{ \AA}$) source and the Bragg–Brentano θ – θ configuration in the $2\theta = 10$ – 80 range, with 0.05° step increment and 3 s acquisition time. The CeO₂ crystallite size was estimated from the Size–Strain plot, as reported in [42]. The “*a*” lattice parameter of ceria was calculated from the eight XRD reflections by Equation (1):

$$a \text{ (\AA)} = \frac{\lambda}{2 \sin \theta} \sqrt{h^2 + k^2 + l^2} \quad (1)$$

The morphologies of CeO₂-NR and the PdO_x/CeO₂-NR were investigated via a Zeiss Sigma 300 VP-FESEM apparatus (20 kV accelerating voltage, 4.0 mm working distance; Carl Zeiss Microscopy, Jena, Germany), equipped with a high-resolution secondary electron in-lens detector, and with EDS. The powder samples were dispersed in isopropyl alcohol followed by 15 min ultrasonication. A thin graphite film was used to place a tiny droplet of sample suspension with approximately 20 μL volume on the sample holder. The EDS analysis was performed in six different areas, and the Pd wt.% was obtained as the mean value.

The N₂ adsorption-desorption isotherms at 77 K were obtained using a Micromeritics Gemini V apparatus (Micromeritics Instrument Corporation, Norcross, GA, USA). Before the N₂ adsorption, the surface was degassed with flowing He at 350 °C for 2 h. The surface area was calculated by the BET method in equilibrium pressure range $p/p^\circ = 0.05$ – 0.20 .

The PSD was calculated by the BJH method from the desorption isotherm; the total pore volume was calculated from the maximum adsorption point $p/p^\circ = 0.98$; the average pore diameter was calculated as (diameter = $4 \times$ Pore Volume/Surface Area) assuming a cylindrical shape of pores.

X-ray Photoelectron Spectroscopy measurements were carried out in an X-ray photoelectron spectrometer of our own construction (home-made instrumentation) with a dual-anode Mg/Al X-ray source, at Mg K-alpha Photon Energy. Measurements were carried out in UHV, and typical vacuum pressure in the analysis chamber during measurements was in the 10^{-9} – 10^{-10} Torr range. Photoelectrons emitted by C1s, O1s, Pd3d, and Ce3d core levels were detected. BEs are reported after correction for charging using the aliphatic C1s as a reference (BE 285.0 eV) [43]. Core level spectra were fitted with a polynomial background and Gaussian peak functions [44,45]. The XPS spectra plotted with peak fitting residuals are reported in Figure S3.

The temperature programmed reduction with hydrogen (H_2 -TPR) was performed by a Thermo Scientific TPDRO1100 (Thermo Fisher Scientific, Waltham, MA, USA) flow apparatus. The H_2 consumption was measured by a TCD calibrated by the reduction of a known mass of CuO (purity 99.99%). A soda lime trap removed the H_2O produced before flowing into the TCD. The sample (0.100 g) was pre-treated in a flow ($20 \text{ cm}^3 \text{ min}^{-1}$) of 10% O_2/He mixture at 400°C for 30 min, and then cooled down. The H_2 -TPR experiment was conducted flowing $30 \text{ cm}^3 \text{ min}^{-1}$ of 5% H_2/Ar mixture. The TCD signal was stabilized flowing the mixture at 40°C for 40 min and then the temperature was increased up to 500°C with a heating rate of $10^\circ\text{C min}^{-1}$; the final temperature was maintained for 60 min.

Catalytic activity of PdO_x/CeO_2 -NR, for solvent-free aerobic oxidation of BnOH derivatives was assessed in a 5 mL two-neck round bottom flask, equipped with reflux condenser and gas inlet and thermometer. A total of 5 mmol of substrate was added to the reaction flask (pre-heated in a silicon oil bath). After the temperature of the substrate was stabilized at the desired value (130°C for 4-hydroxybenzyl alcohol and 4-(benzyloxy)phenol due to their high melting point; 100°C for the rest of the substrates), 5 mg of PdO_x/CeO_2 -NR was added to the flask and 5 mL min^{-1} air flow was bubbled above the reactants. The reactants were constantly stirred during the reaction (500 rpm) to avoid the mass transfer restrictions. The reactions continued for 18 h. Benzophenone was used as internal standard. The conversion of BnOH derivatives, and the selectivity of desired (aldehydic) products are defined in Equations (2) and (3) below:

$$\text{Conversion (\%)} = \frac{\text{moles of substrate reacted}}{\text{initial moles of substrate}} \times 100 \quad (2)$$

$$\text{Selectivity (\%)} = \frac{\text{moles of desired product}}{\text{moles of substrate reacted}} \times 100 \quad (3)$$

Acetonitrile was used to dilute the reactants before being analyzed. The substrates and products were identified by means of GC-MS (Shimadzu VG 70/250S; Kyoto, Japan), using Supelco SLB™ column (30 m, 0.25 mm, and 0.25 μm film thickness; Bellefonte, PA, USA). The program of analysis started at 50°C for 4 min and then the oven was heated by a 10°C/min temperature gradient until reaching 250°C for 10 min. The injector temperature was 250°C .

A HPLC/autosampler/vacuum degasser system (1260 Infinity II, Agilent, Santa Clara, CA, USA) was used for evaluating the results of reactions. The separation was performed on a Luna C18 100 Å column ($4.6 \times 150 \text{ mm}$; $5 \mu\text{m}$; Phenomenex®, Torrance, CA, USA). The mixture of water and acetonitrile (phase A and B respectively) was utilized as the mobile phase, starting from 30% acetonitrile which was linearly increased to 100% within 20 min (flow rate 1 mL min^{-1}).

The catalyst “used” in BnOH oxidation was recovered after the reaction by vacuum filtration, followed by washing with acetonitrile and drying under vacuum in room temperature. The sample was kept in a sealed container before being analyzed by XPS.

4. Conclusions

$\text{PdO}_x/\text{CeO}_2\text{-NR}$ was prepared through wet $\text{Ce}(\text{NO}_3)_3 \cdot 6\text{H}_2\text{O}$ impregnation process using commercial $\text{Pd}(\text{NO}_3)_2$ solution, and subsequent calcination. The Pd-loading process does not affect the crystallite structure and size of $\text{CeO}_2\text{-NR}$ support (excluding any solution of Pd into CeO_2 lattice). As expected, the addition of palladium oxide on the surface causes a decrease of surface area, pore size, and pore volume of the material, suggesting a partial occlusion of ceria pores by PdO_x . The TPR suggests that PdO_x is highly dispersed and strongly interacting with the ceria surface, influencing the ceria redox properties. The XPS evidenced that PdO_x is the only metal oxide species on the ceria surface.

The $\text{PdO}_x/\text{CeO}_2\text{-NR}$, used without pre-reduction, catalyzed the solvent free reactions on benzyl alcohol and its derivatives containing EDG with good to high conversion and selectivity. Derivatives with EWG did not react in these conditions. The more polar environment of the reaction due to the presence of BnOH and the use of PdO_x probably facilitates an ionic mechanism that could explain the high difference of reactivity between substrates containing ERG and EWGs.

During the reaction the in situ partial reduction of the palladium oxide produces a $\text{Pd}(0)/\text{PdO}_x/\text{CeO}_2\text{-NR}$ redox couple stable in the oxidizing condition. We hypothesize that ceria facilitates the redox couple generation and stabilization. The newly formed palladium redox couple was stable in the subsequent runs and even more reactive, confirming the synergistic effect of the simultaneous presence of $\text{Pd}(0)$ and PdO_x in the catalytic process.

Supplementary Materials: The following are available online at <https://www.mdpi.com/article/10.3390/catal13010005/s1>. Figure S1: Evaluation of the average particle dimension of ceria particles by the Size–Strain Plot of XRD diffractions of: (a) $\text{CeO}_2\text{-NR}$; (b) $\text{PdO}_x/\text{CeO}_2\text{-NR}$; Figure S2: Images of (a) calcined $\text{CeO}_2\text{-NR}$, (b) calcined $\text{PdO}_x/\text{CeO}_2\text{-NR}$, (c) used $\text{PdO}_x/\text{CeO}_2\text{-NR}$; Figure S3: XPS spectra, with Peak Fitting Residuals (green curve), of pristine $\text{PdO}_x/\text{CeO}_2\text{-NR}$ (a) Pd3d and (c) Ce3d core levels, and (b) for the “used” $\text{PdO}_x/\text{CeO}_2\text{-NR}$ Pd3d core level.

Author Contributions: Conceptualization, S.S.M. and D.T.; investigation, S.S.M. and S.T.; resources, D.T. and S.T.; data curation, S.S.M., S.T., C.B. and I.L.; writing—original draft preparation, S.S.M., D.T., S.T. and C.B.; writing—review and editing, S.S.M., S.T. and D.T.; funding acquisition, S.T. and D.T. All authors have read and agreed to the published version of the manuscript.

Funding: This work was supported by grants from Ministero dell’Istruzione dell’Università e della Ricerca (MIUR)—Departments of Excellence, 2017—legge 232/2016—art.1, commi 314–337 awarded to Dept. of Science, University Roma Tre, Rome, Italy for 2018–2022.

Data Availability Statement: Data is contained within the article.

Acknowledgments: The authors express appreciation for the kind and generous contribution of Sergio Lo Mastro, Department of Science, Università Roma Tre, for conducting XRD and SEM characterization.

Conflicts of Interest: The authors declare no conflict of interest.

References

1. Giang, L.T.K.; Ku, Y. Selective Oxidation of Benzyl Alcohol in Aqueous Phase by TiO_2 Based Photocatalysts: A Review. *Chem. Eng. Technol.* **2021**, *14*, 2178–2190. [CrossRef]
2. Chan-Thaw, C.E.; Savara, A.; Villa, A. Selective Benzyl Alcohol Oxidation over Pd Catalysts. *Catalysts* **2018**, *8*, 431. [CrossRef]
3. Hu, H.; Xi, J. Single-Atom Catalysis for Organic Reactions. *Chin. Chem. Lett.* **2022**, *2022*, 107959. [CrossRef]
4. Xin, P.; Li, J.; Xiong, Y.; Wu, X.; Dong, J.; Chen, W.; Wang, Y.; Gu, L.; Luo, J.; Rong, H.; et al. Revealing the Active Species for Aerobic Alcohol Oxidation by Using Uniform Supported Palladium Catalysts. *Angew. Chem.* **2018**, *130*, 4732–4736. [CrossRef]
5. Moeini, S.S.; Battocchio, C.; Casciardi, S.; Luisetto, I.; Lupattelli, P.; Tofani, D.; Tuti, S. Oxidized Palladium Supported on Ceria Nanorods for Catalytic Aerobic Oxidation of Benzyl Alcohol to Benzaldehyde in Protic Solvents. *Catalysts* **2019**, *9*, 847. [CrossRef]
6. Moeini, S.S.; Pasqual Laverdura, U.; Marconi, E.; Lisi, N.; Serra, E.; Chierchia, R.; Luisetto, I.; Tuti, S.; Tofani, D. A Novel Pd-P Nano-Alloy Supported on Functionalized Silica for Catalytic Aerobic Oxidation of Benzyl Alcohol. *Catalysts* **2022**, *12*, 20. [CrossRef]
7. Bourbiaux, D.; Mangematin, S.; Djakovitch, L.; Rataboul, F. Selective Aerobic Oxidation of Benzyl Alcohols with Palladium(0) Nanoparticles Suspension in Water. *Catal. Lett.* **2021**, *151*, 3239–3249. [CrossRef]

8. Wang, H.; Kong, W.; Zhu, W.; Wang, L.; Yang, S.; Liu, F. One-Step Synthesis of Pd Nanoparticles Functionalized Crystalline Nanoporous CeO₂ and Their Application for Solvent-Free and Aerobic Oxidation of Alcohols. *Catal. Commun.* **2014**, *50*, 87–91. [[CrossRef](#)]
9. Xia, X.; Liu, S.; Long, Z.; Zhu, W.; Chen, G.; Huang, H.; Tong, M. P,N Co-Doped Biomass Carbon as a Remarkable Metal-Free Catalyst for Solvent-Free Oxidation of Benzyl Alcohol with Ambient Air: The Key Promoting Role of N Co-Doping. *Appl. Surf. Sci.* **2022**, *571*, 151409. [[CrossRef](#)]
10. Li, J.; Wang, Q.; Yu, S.; Wei, Z.; Zhang, H. Highly Dispersed Pd Nanoclusters on Layered Double Hydroxides with Proper Calcination Improving Solvent-Free Oxidation of Benzyl Alcohol. *ACS Sustain. Chem. Eng.* **2022**, *10*, 7223–7233. [[CrossRef](#)]
11. Yi, X.-T.; Li, C.-Y.; Wang, F.; Xu, J.; Xue, B. The Solvent-Free and Aerobic Oxidation of Benzyl Alcohol Catalyzed by Pd Supported on Carbon Nitride/CeO₂ Composites. *New J. Chem.* **2022**, *46*, 7108–7117. [[CrossRef](#)]
12. Nair, V.R.; Maiyalagan, T.; Shendage, S.S. Halloysite Clay Nanotubes with Fe–Al Deposits for the Oxidation of Benzyl Alcohol. *New J. Chem.* **2022**, *46*, 17213–17222. [[CrossRef](#)]
13. Savara, A.; Chan-Thaw, C.E.; Rossetti, I.; Villa, A.; Prati, L. Benzyl Alcohol Oxidation on Carbon-Supported Pd Nanoparticles: Elucidating the Reaction Mechanism. *ChemCatChem* **2014**, *6*, 3464–3473. [[CrossRef](#)]
14. Galvanin, F.; Sankar, M.; Cattaneo, S.; Bethell, D.; Dua, V.; Hutchings, G.J.; Gavriilidis, A. On the Development of Kinetic Models for Solvent-Free Benzyl Alcohol Oxidation over a Gold-Palladium Catalyst. *Chem. Eng. J.* **2018**, *342*, 196–210. [[CrossRef](#)]
15. Han, Q.; Zhou, X.-T.; He, X.-Q.; Ji, H.-B. Mechanism and Kinetics of the Aerobic Oxidation of Benzyl Alcohol to Benzaldehyde Catalyzed by Cobalt Porphyrin in a Membrane Microchannel Reactor. *Chem. Eng. Sci.* **2021**, *245*, 116847. [[CrossRef](#)]
16. Takeyama, T.; Kobayashi, M.; Kikuchi, M.; Ogura, T.; Shimazaki, Y.; Iwatsuki, S. Benzyl Alcohol Oxidation Mechanisms by One- and Two-Electron Oxidized Species of Cu(II)-Salen Complexes with Para-R-Substituents, [Cu(R-Salen)]N⁺ (R = MeO, MeS; n = 1, 2). *Inorg. Chim. Acta* **2020**, *511*, 119848. [[CrossRef](#)]
17. Arena, F.; Gumina, B.; Cannilla, C.; Spadaro, L.; Patti, A.; Spiccia, L. Nanostructured MnO_x Catalysts in the Liquid Phase Selective Oxidation of Benzyl Alcohol with Oxygen: Part II. Reaction Mechanism, Kinetics and Deactivation Pattern. *Appl. Catal. B Environ.* **2015**, *170–171*, 233–240. [[CrossRef](#)]
18. Giannakoudakis, D.A.; Qayyum, A.; Barczak, M.; Colmenares-Quintero, R.F.; Borowski, P.; Triantafyllidis, K.; Colmenares, J.C. Mechanistic and Kinetic Studies of Benzyl Alcohol Photocatalytic Oxidation by Nanostructured Titanium (Hydro) Oxides: Do We Know the Entire Story? *Appl. Catal. B Environ.* **2023**, *320*, 121939. [[CrossRef](#)]
19. Xu, J.; Shang, J.-K.; Chen, Y.; Wang, Y.; Li, Y.-X. Palladium Nanoparticles Supported on Mesoporous Carbon Nitride for Efficiently Selective Oxidation of Benzyl Alcohol with Molecular Oxygen. *Appl. Catal. Gen.* **2017**, *542*, 380–388. [[CrossRef](#)]
20. Grunwaldt, J.-D.; Caravati, M.; Baiker, A. Oxidic or Metallic Palladium: Which Is the Active Phase in Pd-Catalyzed Aerobic Alcohol Oxidation? *J. Phys. Chem. B* **2006**, *110*, 25586–25589. [[CrossRef](#)]
21. Wu, P.; Cao, Y.; Zhao, L.; Wang, Y.; He, Z.; Xing, W.; Bai, P.; Mintova, S.; Yan, Z. Formation of PdO on Au–Pd Bimetallic Catalysts and the Effect on Benzyl Alcohol Oxidation. *J. Catal.* **2019**, *375*, 32–43. [[CrossRef](#)]
22. Tan, H.; Wang, J.; Yu, S.; Zhou, K. Support Morphology-Dependent Catalytic Activity of Pd/CeO₂ for Formaldehyde Oxidation. *Environ. Sci. Technol.* **2015**, *49*, 8675–8682. [[CrossRef](#)] [[PubMed](#)]
23. Jürgensen, A.; Heutz, N.; Raschke, H.; Merz, K.; Hergenröder, R. Behavior of Supported Palladium Oxide Nanoparticles under Reaction Conditions, Studied with near Ambient Pressure XPS. *Anal. Chem.* **2015**, *87*, 7848–7856. [[CrossRef](#)] [[PubMed](#)]
24. Thommes, M.; Kaneko, K.; Neimark, A.V.; Olivier, J.P.; Rodríguez-Reinoso, F.; Rouquerol, J.; Sing, K.S.W. Physisorption of Gases, with Special Reference to the Evaluation of Surface Area and Pore Size Distribution (IUPAC Technical Report). *Pure Appl. Chem.* **2015**, *87*, 1051–1069. [[CrossRef](#)]
25. Shyu, J.Z.; Weber, W.H.; Gandhi, H.S. Surface Characterization of Alumina-Supported Ceria. *J. Phys. Chem.* **1988**, *92*, 4964–4970. [[CrossRef](#)]
26. Szijjártó, G.P.; Pászti, Z.; Sajó, I.; Erdőhelyi, A.; Radnóczy, G.; Tompos, A. Nature of the Active Sites in Ni/MgAl₂O₄-Based Catalysts Designed for Steam Reforming of Ethanol. *J. Catal.* **2013**, *305*, 290–306. [[CrossRef](#)]
27. Danielis, M.; Betancourt, L.E.; Orozco, I.; Divins, N.J.; Llorca, J.; Rodríguez, J.A.; Senanayake, S.D.; Colussi, S.; Trovarelli, A. Methane Oxidation Activity and Nanoscale Characterization of Pd/CeO₂ Catalysts Prepared by Dry Milling Pd Acetate and Ceria. *Appl. Catal. B Environ.* **2021**, *282*, 119567. [[CrossRef](#)]
28. Gopinath, R.; Lingaiah, N.; Sreedhar, B.; Suryanarayana, I.; Sai Prasad, P.S.; Obuchi, A. Highly Stable Pd/CeO₂ Catalyst for Hydrodechlorination of Chlorobenzene. *Appl. Catal. B Environ.* **2003**, *46*, 587–594. [[CrossRef](#)]
29. Kwon, G.; Kim, G.; Lee, H. Continuous Methane to Ethane Conversion Using Gaseous Oxygen on Ceria-Based Pd Catalysts at Low Temperatures. *Appl. Catal. Gen.* **2021**, *623*, 118245. [[CrossRef](#)]
30. Fan, L.; Zhang, J.; Ma, K.; Zhang, Y.; Hu, Y.-M.; Kong, L.; Jia, A.; Zhang, Z.; Huang, W.; Lu, J.-Q. Ceria Morphology-Dependent Pd-CeO₂ Interaction and Catalysis in CO₂ Hydrogenation into Formate. *J. Catal.* **2021**, *397*, 116–127. [[CrossRef](#)]
31. Yan, Z.; Tomer, A.; Perrussel, G.; Ousmane, M.; Katryniok, B.; Dumeignil, F.; Ponchel, A.; Liebens, A.; Pera-Titus, M. A Pd/CeO₂ “H₂ Pump” for the Direct Amination of Alcohols. *ChemCatChem* **2016**, *8*, 3347–3352. [[CrossRef](#)]
32. Luo, M.-F.; Hou, Z.-Y.; Yuan, X.-X.; Zheng, X.-M. Characterization Study of CeO₂ Supported Pd Catalyst for Low-Temperature Carbon Monoxide Oxidation. *Catal. Lett.* **1998**, *50*, 205–209. [[CrossRef](#)]
33. Luo, J.-Y.; Meng, M.; Xian, H.; Tu, Y.-B.; Li, X.-G.; Ding, T. The Nanomorphology-Controlled Palladium-Support Interaction and the Catalytic Performance of Pd/CeO₂ Catalysts. *Catal. Lett.* **2009**, *133*, 328–333. [[CrossRef](#)]

34. Neal, L.M.; Everett, M.L.; Hoflund, G.B.; Hagelin-Weaver, H.E. Characterization of Palladium Oxide Catalysts Supported on Nanoparticle Metal Oxides for the Oxidative Coupling of 4-Methylpyridine. *J. Mol. Catal. Chem.* **2011**, *335*, 210–221. [[CrossRef](#)]
35. Kara, G.K.; Rahimi, J.; Niksefat, M.; Taheri-Ledari, R.; Rabbani, M.; Maleki, A. Preparation and Characterization of Perlite/V₂O₅ Nano-Spheres via a Novel Green Method: Applied for Oxidation of Benzyl Alcohol Derivatives. *Mater. Chem. Phys.* **2020**, *250*, 122991. [[CrossRef](#)]
36. Cheng, C.; Wang, J.; Shen, D.; Xue, J.; Guan, S.; Gu, S.; Luo, K.H. Catalytic Oxidation of Lignin in Solvent Systems for Production of Renewable Chemicals: A Review. *Polymers* **2017**, *9*, 240. [[CrossRef](#)]
37. Higashimoto, S.; Kitao, N.; Yoshida, N.; Sakura, T.; Azuma, M.; Ohue, H.; Sakata, Y. Selective Photocatalytic Oxidation of Benzyl Alcohol and Its Derivatives into Corresponding Aldehydes by Molecular Oxygen on Titanium Dioxide under Visible Light Irradiation. *J. Catal.* **2009**, *266*, 279–285. [[CrossRef](#)]
38. Goksu, H.; Sen, F. Handy and Highly Efficient Oxidation of Benzylic Alcohols to the Benzaldehyde Derivatives Using Heterogeneous Pd/AlO(OH) Nanoparticles in Solvent-Free Conditions. *Sci. Rep.* **2020**, *10*, 5731. [[CrossRef](#)]
39. Wang, Z.; Zhang, B.; Yang, S.; Yang, X.; Meng, F.; Zhai, L.; Li, Z.; Zhao, S.; Zhang, G.; Qin, Y. Dual Pd²⁺ and Pd⁰ Sites on CeO₂ for Benzyl Alcohol Selective Oxidation. *J. Catal.* **2022**, *414*, 385–393. [[CrossRef](#)]
40. NIST X-ray Photoelectron Spectroscopy Database, Version 4.1. Available online: <https://srdata.nist.gov/xps/> (accessed on 13 November 2022).
41. Japa, M.; Tantraviwat, D.; Phasayavan, W.; Nattestad, A.; Chen, J.; Inceesungvorn, B. Simple Preparation of Nitrogen-Doped TiO₂ and Its Performance in Selective Oxidation of Benzyl Alcohol and Benzylamine under Visible Light. *Colloids Surf. A Physicochem. Eng. Asp.* **2021**, *610*, 125743. [[CrossRef](#)]
42. Tuti, S.; Luisetto, I.; Pasqual Laverdura, U.; Marconi, E. Dry Reforming of Methane on Ni/Nanorod-CeO₂ Catalysts Prepared by One-Pot Hydrothermal Synthesis: The Effect of Ni Content on Structure, Activity, and Stability. *Reactions* **2022**, *3*, 333–351. [[CrossRef](#)]
43. Moulder, J.F.; Stickle, W.F.; Sobol, P.E.; Bomben, K.D. *Handbook of X-ray Photoelectron Spectroscopy: A Reference Book of Standard Spectra for Identification and Interpretation of XPS Data*; Chastain, J., King, R.C., Jr., Eds.; Physical Electronics Division, Perkin-Elmer Corporation: Eden Prairie, MN, USA, 1992; ISBN 978-0-9627026-2-4.
44. Shirley, D.A. High-Resolution X-ray Photoemission Spectrum of the Valence Bands of Gold. *Phys. Rev. B* **1972**, *5*, 4709–4714. [[CrossRef](#)]
45. Hantsche, H. High Resolution XPS of Organic Polymers, the Scienta ESCA300 Database. By G. Beamson and D. Briggs, Wiley, Chichester 1992, 295 pp., Hardcover, ISBN 0-471-93592-1. *Adv. Mater.* **1993**, *5*, 778. [[CrossRef](#)]

Disclaimer/Publisher's Note: The statements, opinions and data contained in all publications are solely those of the individual author(s) and contributor(s) and not of MDPI and/or the editor(s). MDPI and/or the editor(s) disclaim responsibility for any injury to people or property resulting from any ideas, methods, instructions or products referred to in the content.